SUPPORTING INFORMATION

Proteolytic Activity at Quantum Dot-Conjugates: Kinetic Analysis Reveals Enhanced Enzyme Activity and Localized Interfacial "Hopping"

W. Russ Algar[a,c], Anthony Malonoski[a], Jeffrey R. Deschamps[a], Juan B. Blanco-Canosa[d], Kimihiro Susumu[b], Michael H. Stewart[b], Brandy J. Johnson[a], Philip E. Dawson[d] and Igor L. Medintz[a]

[a] Center for Bio/Molecular Science and Engineering, Code 6900
[b] Optical Sciences Division, Code 5611
U.S. Naval Research Laboratory
Washington, DC 20375, USA.

[c] College of Science
George Mason University
Fairfax, VA 22030, USA.

[d] Departments of Cell Biology and Chemistry
The Scripps Research Institute
La Jolla, CA 92037, USA.

Corresponding author:
Igor L. Medintz
Center for Bio/Molecular Science and Engineering
U.S. Naval Research Laboratory Code 6900
4555 Overlook Ave, SW
Washington D.C., 20375
Ph: 202-404-6046
Fax: 202-767-9594
Igor.medintz@nrl.navy.mil

Table of Contents

Detailed Materials and Methods **3**
- Enzyme 3
- Instruments 3
- Peptide Labeling 3
- Preparation of 2-naphthylamine calibration samples 3
- Preparation of pre-digested peptide (product fragment) samples 3
- MM plot for trypsin catalyzed hydrolysis of BANA 4
- MM plot for trypsin catalyzed hydrolysis of peptide substrate 4
- Kinetic assays with BANA 5
- Kinetic assays with QD-peptide substrate conjugates 5
- Gel electrophoresis 6

Data Analysis **6**
- FRET calculations 6
- Kinetic analysis of QD-FRET assays 8
- Kinetic analysis of BANA assays 9

Design of the Peptide Substrate and Structural Simulation **9**

Spectral Overlap Integrals and Förster Distances **12**

Validation with BANA substrate **13**
- MM plot analysis 13
- Kinetic analysis 13

Non-specific adsorption and FRET calibration curves **15**

Digestion of Peptide Substrates and Kinetic Analysis **18**

Digestion of Peptide Substrates and a Classic MM Plot **18**

Digestion of Quantum Dot-Peptide Substrate Conjugates **19**

References **24**

Detailed Materials and Methods

Enzyme

Trypsin from bovine pancreas (MW 23.8 kDa, 12 705 BAEE units/mg protein, 12 705 BAEE units/mg solid, foreign chymotrypsin activity 0.67 BTEE units/mg protein; EC number 3.4.21.4; derived from New Zealand sourced pancreas, ethanol precipitate) was purchased from Sigma-Aldrich (St. Louis, MO). Note: BAEE is N_{α}-benzoyl-L-arginine ethyl ester; BTEE is N_{α}-tyrosine-L-arginine ethyl ester.

Instruments

PL measurements were made using either a Tecan (Durham, NC) Sapphire or Tecan Infinite M1000 fluorescence multifunction plate reader.

Peptide Labeling

A mass of *ca.* 1 mg of peptide was dissolved in 1 mL of phosphate buffered saline (PBS; 137 mM NaCl, 10 mM phosphate, 2.7 mM KCl, pH 7.4), and combined with excess Cy3-maleimide monoreactive dye (GE Healthcare, Piscataway, NJ) or A594-maleimide (Invitrogen by Life Technologies, Carlsbad, CA) at room temperature for 1–2 h and then left overnight at 4°C. Excess unreacted dye was initially removed by loading the reaction onto three consecutive 0.5 mL columns of Ni^{2+}-nitrilotriacetic acid (Ni-NTA) agarose media (Qiagen Valencia, CA). Columns with bound peptide were washed with PBS, and the labeled peptide eluted with 300 mM imidazole in PBS. Cy3-labeled peptide was desalted and the imidazole removed using a reverse-phase oligonucleotide purification cartridge (OPC; Applied Biosystems, Foster City, CA) and washes with 0.1 M triethylamine acetate buffer. Labeled peptide was eluted using 1 mL of 70% acetonitrile in doubly-distilled deionized H_2O. Purified Cy3-peptide was quantitated by UV-visible spectroscopy using the Cy3 (ε = 150 000 M^{-1} cm^{-1} at 550 nm) and A594 (ε = 73 000 M^{-1} cm^{-1} at 590 nm) absorbance peaks, then aliquoted, dried, and stored at −20 °C prior to use. This protocol has been described in detail elsewhere.[1]

Preparation of 2-naphthylamine calibration samples

2-Naphthylamine samples were prepared from the hydrolysis of the corresponding concentration of BANA using 1.4 µM trypsin at 37 ˚C for 4 h, and then left at 22 ˚C for 1.5 h.

Preparation of pre-digested peptide (product fragment) samples

Equal volumes of Cy3/A594-labeled peptide substrate (50 µM) and trypsin (8.6 µM) were mixed and left overnight at room temperature. These solutions were used for calibrations with *only* digested product fragments. For the mixed calibration with *both* A594-labeled substrate and digested product fragment (*vide infra*), residual trypsin activity in the solution (800 µL, 25 µM)

was first inhibited with 4-(2-Aminoethyl) benzenesulfonyl fluoride hydrochloride (AEBSF) as part of a protease inhibitor cocktail (100 μL DMSO; Sigma-Aldrich).

MM plot for trypsin catalyzed hydrolysis of BANA

Dilutions of BANA (50 μL, 0–1000 μM) were prepared in 1X PBS. Digestions were initiated by adding trypsin (50 μL, 86 nM) to the BANA samples, and the evolution of 2-naphthylamine fluorescence monitored at 415 nm (excitation 290 nm) at 2.5 min intervals. Note that the fluorescence from the BANA substrate was negligible relative to that of the 2-naphthylamine product (an equal amount of BANA had <0.5% the PL intensity of 2-naphtylamine at 415 nm). The time dependent 2-naphthylamine product concentration during BANA hydrolysis was determined, and the initial reaction rate estimated from the approximately linear progress over the first 30 min of hydrolysis. Fitting the MM plot (Fig. 3) to manuscript Eqn. 3 was used to derive K_m, V, and k_{cat}. In parallel with these samples, dilutions of 2-naphthylamine (100 μL, 1–125 μM) from pre-hydrolysis of BANA were measured and provided time-dependent calibration functions that correlated PL intensity to product concentration.

MM plot for trypsin catalyzed hydrolysis of peptide substrate

The peptide substrate was labeled with Alexa Fluor 568 (A568) (analogous to A594) and quantitated (ε_{578} = 91 000 M^{-1} cm^{-1}). Dilutions of the peptide in the range of 0–2000 μM in PBS were prepared, and aliquots (10 μL from 20 μL) set aside for a calibration curve. Digestion was initiated by adding trypsin (10 μL, 258 nM). The reaction was allowed to proceed for 20 min at 22 °C prior to adding protease inhibitor cocktail (10 μL in DMSO; Sigma-Aldrich) containing AEBSF. Ni-NTA-agarose resin (suspended in ethanol; Qiagen, Valencia, CA) was added to the inhibited reaction mixture. In separate experiments, the added quantity of resin was confirmed to be sufficient to bind the total quantity of substrate peptide. The samples were then diluted (to 600 μL using 1X PBS), centrifuged, and an aliquot of the supernatant collected for fluorescence measurements. The collected supernatant was centrifuged prior to loading into a microtiter plate. The supernatant contained product as fluorescently labeled, digested peptide fragments; the resin retained undigested, dye-labeled substrate peptides *via* their polyhistidine tail. The calibration aliquots set aside previously were diluted by the same factor using the same solvent composition (65% 1X PBS, 33% ethanol, 2% DMSO) and their fluorescence measured in parallel. The product concentrations, which were derived from the calibration aliquots, were converted to initial rates, and a MM plot of initial velocity *versus* substrate concentration was fit with Eqn. 3 to derive values for K_m, V, and k_{cat}. Fig. S1 illustrates the assay format.

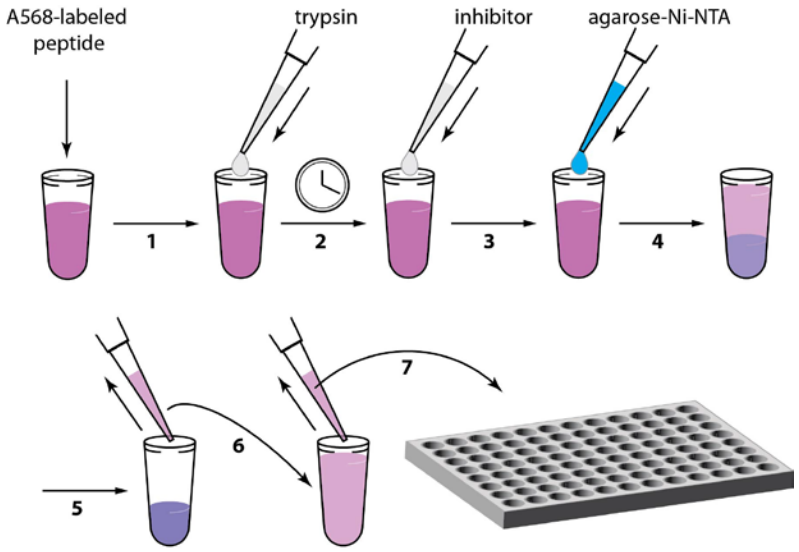

Figure S1. Schematic protocol for determining the Michaelis-Menten kinetic parameters for tryptic digestion of dye-labeled (A568) substrate peptide: (1) addition of trypsin; (2) digestion for 20 min followed by addition of inhibitor; (3) addition of agarose-Ni-NTA resin; (4) mixing and centrifugation; (5) collection of supernatant containing product peptide fragments; (6) transfer and centrifugation; (7) loading into a microtiter plate for fluorescence measurements.

Kinetic assays with BANA

A series of dilutions of trypsin (50 µL at 0–5.5 µM) in 1X PBS were prepared in a 96-well plate in triplicate. Hydrolysis reactions were initiated by adding BANA (50 µL, 116 µM) in 1X PBS to each well. The evolution of fluorescence from the 2-naphthylamine product at 415 nm (excitation at 290 nm) was monitored at 2.5 min intervals. Calibrations samples of 2-naphthylamine from pre-hydrolyzed BANA (100 µL, 0.25–125 µM) were measured in parallel and provided time-dependent calibration functions that correlated PL intensity to product concentration. An analogous experiment was done by initiating hydrolysis with a BANA solution (116 µM) that also contained QDs (1 µM), and parallel calibration samples of 2-naphthylamine from pre-hydrolyzed BANA (0.13–63 µM) and QDs (0.5 µM). Both experiments were run concurrently in the same microtiter plate.

Kinetic assays with QD-peptide substrate conjugates

A series of trypsin dilutions (50 µL at 0, 1.3 (n = 2.4 only), 2.7, 5.4, 11, 22, 43, 86, 172, 343, 687, 1373 nM) in 1X PBS were prepared in triplicate. Hydrolysis reactions were initiated by adding QD-peptide substrate conjugate (50 µL, 1 µM) in 1X PBS to the trypsin dilutions. All experiments were done at *ca.* 22 °C. The QD-peptide substrate conjugates added to the trypsin dilutions were prepared as a single batch (> 600 pmol) for a given conjugate valence. The PL of each well was measured serially at 530 nm (QD) and 575/617 nm (Cy3/A594) with excitation at 400/450 nm (QD-Cy3/QD-A594) every 2.5 min over at least 2 h. The A/D PL ratio was determined from these PL intensities.

Gel electrophoresis

Gradient (8–25%) polyacrylamide gel electrophoresis was run on A594-labeled peptide substrate and pre-digested A594-labeled peptide product using a Pharmacia LKB PhastSystem and PhastGel SDS Buffer Strips (GE Healthcare, Piscataway, NJ) according to the manufacturer's protocol. Peptides were dissolved at *ca.* 5 µM. The gel was imaged under UV illumination using a 540–600 nm optical bandpass filter.

A 1.5% agarose gel was cast with 1X TBE buffer and *ca.* 15 µL replicate samples of 0.5 µM QDs, 0.5 µM QD-(peptide-A594)$_{13}$ conjugate, and 0.5 µM QD-(peptide-A594)$_{13.4}$ conjugate digested by 687 nM trypsin were loaded into the wells. The peptide conjugates were prepared by self-assembly over 1 h, and trypsin digestion was over 3 h at room temperature. The gel was run for ~15 min at *ca.* 10 V cm^{-1} and then imaged twice under UV illumination: once using a 485–600 nm optical bandpass filter (QD PL) and once using a 540–600 nm optical bandpass filter (A594 PL). The two images were merged into a pseudocolor image using Image J software (National Institutes of Health, Bethesda, MD).

Data Analysis

FRET calculations

Spectral overlap integrals, J (mol^{-1} cm^6) were calculated using Eqn. S1, where $F(\lambda)$ is the donor PL spectrum normalized to unit area, $\varepsilon(\lambda)$ is the wavelength-dependent acceptor extinction coefficient (cm^2 mol^{-1}), and λ is the wavelength (cm). The Förster distances, R_0, were calculated using Eqn. S2, where n is the refractive index of the medium, Φ_D is the donor quantum yield, and κ^2 is the dipole orientation factor.[2] A value of 2/3 was used for κ^2 and is appropriate for these randomly assembled, centrosymmetric, QD donor-multiple acceptor configurations.[3]

$$J(\lambda) = \int F(\lambda)\varepsilon(\lambda)\lambda^4 \, d\lambda \tag{S1}$$

$$R_0^6 = \left(8.79 \times 10^{-28} \text{ mol}\right) n^{-4} \Phi_D \kappa^2 J \tag{S2}$$

The A/D PL ratio, ρ, was calculated according to Eqn. S3. The notations D and A refer to the QD donor and dye acceptor, respectively. The notations DA and AD refer to measurements of donor and acceptor PL, respectively, in a FRET paired system. The terms λ_D and λ_A refer to emission wavelengths (nm) predominately associated with the donor or acceptor (λ_{QD} = 530, λ_{Cy3} = 575, λ_{A594} = 617). The α terms are peak area-to-height corrections that scale the single wavelength PL intensities to match the area of the corresponding full PL spectrum. The σ term corrects for the QD donor crosstalk at the acceptor measurement wavelength, and is scaled according to the measured QD peak height. The values of the correction parameters (derived from experimental spectra) were $\alpha_{QD,\,530} \approx 46$, $\alpha_{Cy3,\,575} \approx 58$, $\alpha_{A594,\,617} \approx 55$, $\sigma_{QD,\,575} = 0.06$ and $\sigma_{QD,\,617} = 0.01$.

$$\rho = \frac{I_{\mathrm{AD}}}{I_{\mathrm{DA}}} = \frac{\alpha_{\mathrm{A},\lambda_D}\left[\left(I_{\mathrm{AD},\lambda_A} - I_{\mathrm{A},\lambda_A}\right) - \sigma_{\mathrm{D},\lambda_A} I_{\mathrm{DA},\lambda_D}\right]}{\alpha_{D,\lambda_D} I_{\mathrm{DA},\lambda_D}} \tag{S3}$$

The FRET efficiency (Eqn. 1), E_{FRET}, can potentially be determined from the ratio of acceptor and donor PL. This requires that the acceptor has a non-trivial quantum yield, and its direct excitation is negligible (or accounted for) in FRET experiments. Donor and acceptor PL intensities are determined by the probability of excitation and efficiency of PL, such that I_{AD} and I_{DA} can be expressed as Eqn. S4, where ε_{D} and ε_{A} are the molar absorption coefficients at the excitation wavelength, Φ_{D} and Φ_{A} are the PL quantum yields, and c_{D} and c_{A} their respective concentrations. Since the interest is in the A/D PL ratio, and consistent, narrow band excitation is used, it is not necessary to include terms for the instrument collection efficiency, excitation source intensity, or optical path length. I_{AD} is the sum of directly excited acceptor PL, $I_{\mathrm{A,dir}}$, and FRET-sensitized acceptor PL, $I_{\mathrm{A,FRET}}$.

$$\frac{I_{\mathrm{AD}}}{I_{\mathrm{DA}}} = \frac{I_{\mathrm{A,dir}} + I_{\mathrm{A,FRET}}}{I_{\mathrm{DA}}} = \frac{\varepsilon_{\mathrm{A}}\Phi_{\mathrm{A}}c_{\mathrm{A}} + \left(\varepsilon_{\mathrm{D}}c_{\mathrm{D}}E_{FRET}\right)\Phi_{\mathrm{A}}}{\varepsilon_{\mathrm{D}}\Phi_{\mathrm{D}}c_{\mathrm{D}}\left(1 - E_{FRET}\right)} \tag{S4}$$

If direct excitation of the acceptor is negligible ($\varepsilon_{\mathrm{A}} \rightarrow 0$) then Eqn. S4 simplifies to Eqn. S5, which can be rearranged to give Eqn. S6, the FRET efficiency in terms of the acceptor/donor PL ratio, $I_{\mathrm{AD}}/I_{\mathrm{DA}}$, and without a donor-only reference state.

$$\frac{I_{\mathrm{AD}}}{I_{\mathrm{DA}}} = \frac{E_{\mathrm{FRET}}\Phi_{\mathrm{A}}}{\Phi_{\mathrm{D}}\left(1 - E_{\mathrm{FRET}}\right)} \tag{S5}$$

$$E_{\mathrm{FRET}} = \frac{\left(I_{\mathrm{AD}}/I_{\mathrm{DA}}\right)}{\left(\Phi_{\mathrm{A}}/\Phi_{D}\right) + \left(I_{\mathrm{AD}}/I_{\mathrm{DA}}\right)} \tag{S6}$$

When direct excitation of acceptor is not negligible, $I_{\mathrm{A,dir}}$ can be estimated experimentally and used to determine $I_{\mathrm{A,FRET}}$. Equating Eqn. 1 and Eqn. S6 leads to the relationship between the A/D PL ratio, $I_{\mathrm{AD}}/I_{\mathrm{DA}}$, and the number of acceptors per QD donor, a, shown in Eqn. S7. In real experiments, deviations from linearity may be observed as the number acceptors increases due to changes in the acceptor quantum yield, Φ_{A}, other dye properties, or donor-acceptor distance, r. Nonetheless, this relation illustrates that the A/D PL ratio is correlated to conjugate valence for QD-substrate peptide assemblies.

$$\left(I_{\mathrm{AD}}/I_{\mathrm{DA}}\right) = n\left(\Phi_{\mathrm{A}}/\Phi_{\mathrm{D}}\right)\left(R_0/r\right)^6 \tag{S7}$$

In Fig. 2, the plot of A594/QD PL ratio as a function of n is approximately linear, in agreement with Eqn. S7, while the Cy3/QD PL ratio was weakly quadratic. The latter may be consequence of increases in Cy3 quantum yield as local viscosity increases[4] with greater values of n.

Kinetic analysis of QD-FRET assays

As noted earlier, the A/D PL ratio at each time point in the assay was determined from the measured intensities at 530 nm and 575/617 nm, which were processed according to Eqn. S3. To partially correct for wavelength-dependent drift in the experiments, the time- and enzyme-dependent A/D PL ratio, $\rho_{t,[E]}$, was normalized to the control sample, with $[E]_0 = 0$ nM. This was done using Eqn. S8, where $(I_{AD}/I_{DA})_{i,[E]}$ is the A/D PL ratio for QD-peptide substrate conjugate being digested by $[E]_0$ trypsin at the i^{th} of T total time dependent measurements, and $(I_{AD}/I_{DA})_{i,0\ nM}$ is the corresponding data for the control sample. The bracketed term in Eqn. S8 is the time-averaged A/D PL ratio for the control sample.

$$\left(I_{AD}/I_{DA}\right)_{i,[E]_0} = \frac{\left(I_{AD}/I_{DA}\right)_{i,[E]_0}}{\left(I_{AD}/I_{DA}\right)_{i,0\ nM}}\left(\frac{1}{T}\sum_{j=0}^{T}\left(I_{AD}/I_{DA}\right)_{j,0\ nM}\right) \tag{S8}$$

The normalized data was converted to the time time-dependent QD-substrate conjugate valence, n_t, using the empirical A/D PL ratio calibrations, then converted to the time-dependent substrate concentration, $[S]_t = n_t[QD] = 0.5n_t$ μM. These latter curves were then converted into enzyme-time, t_E, data by multiplying the time point, t (s), by the enzyme concentration, $[E]_0$ (μM), as $t = [E]_0 t$.

Since Eqn. 4 does not provide an explicit relation between $[S]_t$ and t, $[S]_t$ must be expressed in an alternative closed form according to Eqn. S9.[5] Unfortunately, Eqn. S9 uses the Lambert W function (*a.k.a.* Omega function), which most fitting programs are not capable of handling; however, approximate solutions of the Lambert function have been derived in terms of functions that are suitable for most fitting programs.[5, 6] We use the expression[5] defined by Eqns. S10–S11 to fit reaction progress curves in enzyme-time using the Levenberg-Marquardt method for non-linear regression in *pro Fit* software (Ver. 6.2.2, Quantum Soft, Switzerland). The value of $[S]_0$ was taken from the experimental data, k_{cat} was assumed to be that determined for peptide substrate in bulk solution, and K_m was left as the fitting parameter. The values of $K_{m,\,eff}$ in Table 1 were obtained by fitting only the initial decay of the progress curves in Fig. 4. so as to avoid influence from the departure of the curves from the classic MM trajectory at latter enzyme-times.

$$[S]_t = K_m \cdot W\left\{\frac{[S]_0}{K_m}\exp\left(\frac{[S]_0 - k_{cat}[E]_0 t}{K_m}\right)\right\} \tag{S9}$$

$$[S]_t = \frac{1}{K_m}\left(1.4586887\ln\left[\frac{1.2z}{\ln\left(\frac{2.4z}{\ln(1+2.4z)}\right)}\right] - 0.4586887\ln\left[\frac{2z}{\ln(1+2z)}\right]\right) \tag{S10}$$

$$z = \left([S]_0/K_m\right)\exp\left[K_m^{-1}\left([S]_0 - k_{cat}t_E\right)\right] \tag{S11}$$

Kinetic analysis of BANA assays

The kinetic analysis of BANA hydrolysis assays was done analogously to that described above for the QD-FRET assays with QD-peptide substrate conjugates. The only exception was the conversion of PL data into substrate concentration. Rather than A/D PL ratios, the hydrolysis assays directly measured $[P]_t$ from fluorescence intensity, with parallel time-dependent calibration curves with 2-naphthylamine from pre-digested BANA. From the initial concentration of BANA, $[S]_t$ was calculated from $[P]_t$ and Eqns. S9–S11 applied.

Design of the Peptide Substrate and Structural Simulation

The trypsin substrate was a modular peptide designed for use in this study: C-STRIDEANQAAT-SLP_7S-H_6 (MW *ca.* 3.2 kDa). The STRIDEANQAAT module originates from the sequence SNKTRIDEANQRATKM, which constitutes residues 187–202 of the synaptosomal-associated protein 25 (SNAP-25).[7, 8] This sequence can assume a highly bent or kinked structure and is specifically cleaved by the *Clostridial botulinum* neurotoxin light chain A protease. A slightly modified version of this peptide sequence was also found to be highly responsive to trypsin activity as a QD-conjugate.[1, 9] For this study, the original sequence was modified to display only a single arginine residue that acted as a unique cleavage site. The bent motif was retained and expected to bring the acceptor dye back in close proximity to the QD surface, thereby improving relative FRET efficiency. The adjacent SLP_7S sequence incorporated a polyproline motif that forms a type II helix and functions as an extended spacer with a predicted linear extension of ~14 Å.[10] Serine and lysine residues were inserted for additional length and flexibility, helping to ensure that the STRIDEANQAAT sequence extended away from the QD surface. A model of the predicted peptide structure in solution is shown in Fig. S2. Note the similarity to that of the QD assembled peptide conformation.

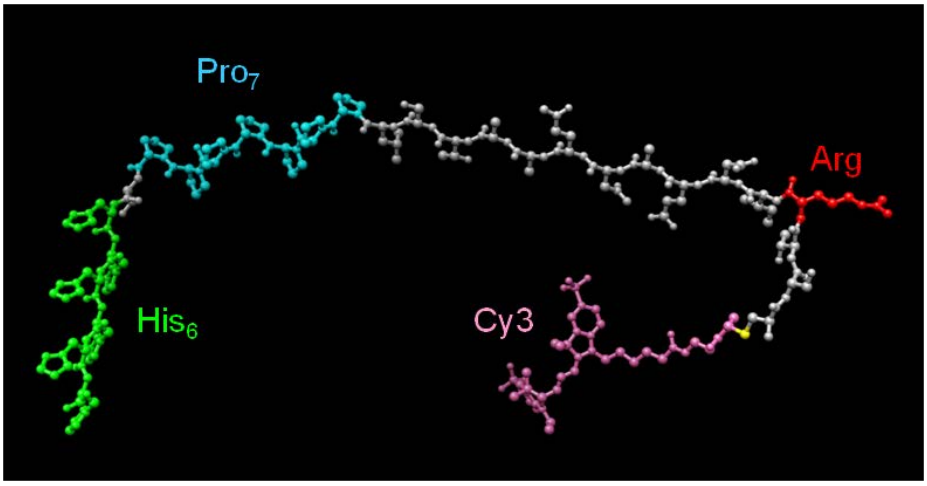

Figure S2. Structural representation of the Cy3 labeled peptide substrate, illustrating a bent or kinked structure. The polyhistidine and polyproline tracts are highlighted along the length of the peptide, as is the arginine cleavage site. Conjugation of the Cy3 at the thiol of the terminal cysteine is indicated in yellow.

All structures were created using tools in UCSF Chimera, version 1.4.1.[11] The general methods we describe here have been applied with other QD-conjugated peptide, protein, and DNA systems previously.[9, 12-19] Energy minimization was carried out in Chimera using built in features, including ANTECHAMBER (version 1.27) and the AM1-BCC method of calculating charges.[20] The structure for trypsin is PDB entry 1YF4.[21] The conformation of the modular peptide in the trypsin binding pocket was modeled using a peptide inhibitor bound to bovine trypsin, PDB entry 2O9Q.[22] Fig. 6 shows the modular peptide bound to a 5.6 nm diameter QD. The translucent shell defines the space occupied by the PEG (QD + 38Å). For illustrative purposes torsion angles in the peptide were adjusted to achieve the 5.1 nm spacing observed for the complex by FRET. Note that this places the enzyme and the binding region of the peptide outside of the PEG region.

The model peptide structure was then imported into ChemBio3D Ultra (version 11.0, CambridgeSoft, Inc.) and a global energy minimization performed using MM2. The effect of conformation on the minimum energy was examined by altering two torsion angles at the junction between the polyproline helix and the *N*-terminal region of the peptide and plotting the minimized energy for all conformations. This resulted in three regions of local minimum energy: one with a *trans*-peptide bond, **1**, one with a *cis*-peptide bond, **2**, and a third with the bent conformation, **3** (Fig. S3A). The minimized energies of these three conformations were within 1 kcal/mol. The energy barrier between conformations **1** and **2** (*i.e.* the *trans* and *cis* conformations) was approximately 21 kcal/mol while the barriers between conformations **1** and **3**, and conformations **2** and **3** were 17 and 26 kcal/mol respectively.

To determine if the energy required to transition from a *cis*-to-*trans* configuration at the *N*-terminal end of the polyproline helix was representative of a *cis*-to-*trans* transition within the helix, this same calculation was performed between residues 18 and 19 (*i.e.* near the middle of the polyproline helix, see Fig. S3B). In this case (kinking of the helix) larger differences were found between the local energy minima. The lowest energy conformer had a tight fold that maximized intra-molecular interactions. This conformation, **4b**, had a minimized energy 10 kcal/mol lower than the next lowest energy conformer, a *cis*-peptide bond, **2b**. The energy was also 13 kcal/mol lower than the folded conformation, **3b**, and 18 kcal/mol lower than the trans-peptide bond, **1b**. Comparing these conformations to those at the end of the polyproline helix,

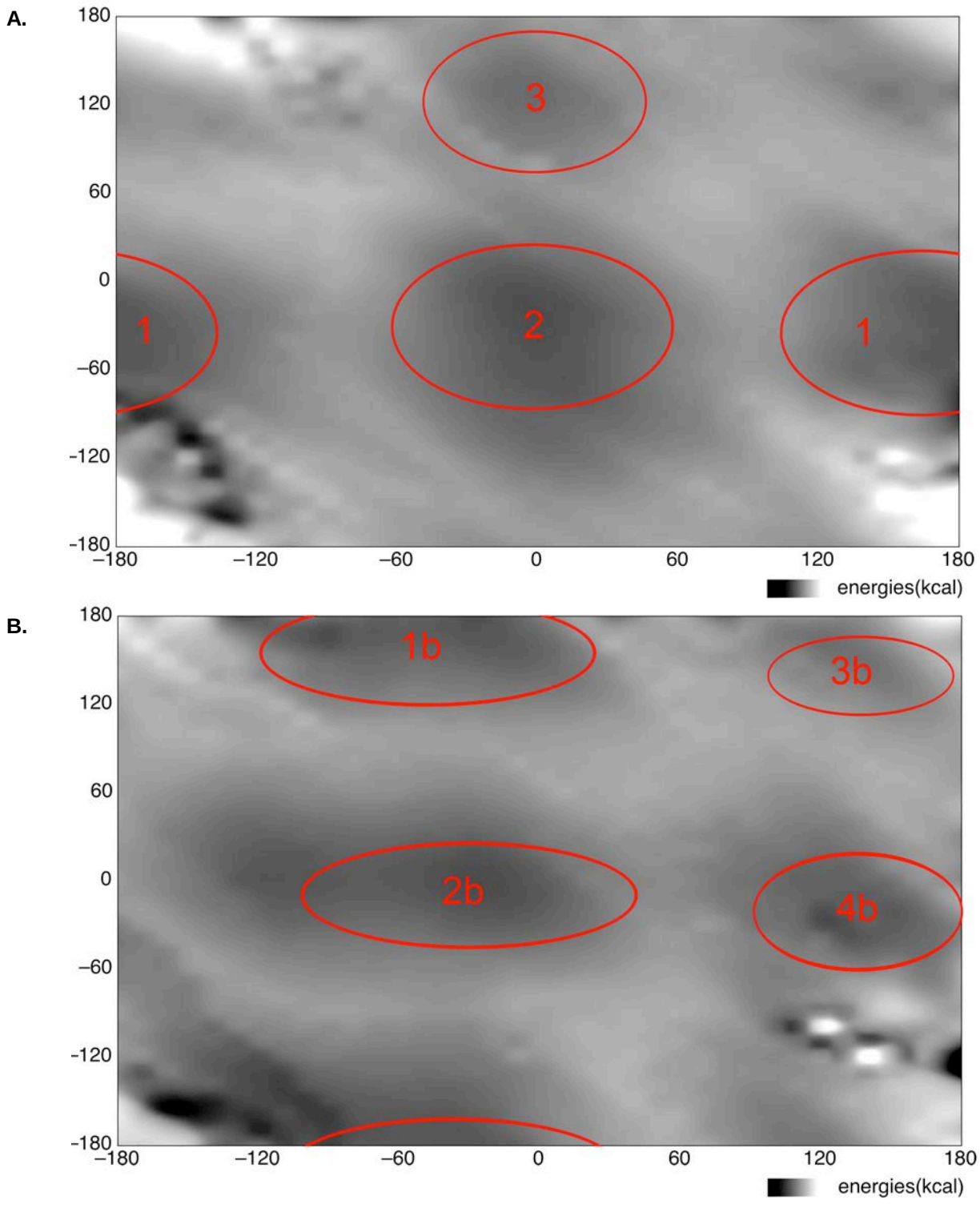

Figure S3. (A) Minimum energy from peptide model while adjusting torsion angles at the junction between the polyproline region and the N-terminal region. **(B)** Minimum energy from peptide model while adjusting torsion angles within the polyproline region to create a kink in the helix. The black regions in (A) and (B) represent unrealistic structures.

the energy barrier between conformations **1b** & **2b** (*i.e.* the *trans* and *cis* conformations) was approximately 29 kcal/mol, while the barriers between conformations **1b** & **3b** and conformations **2b** & **3b** were 22 and 25 kcal/mol, respectively. Conformation **4b** was not considered since no similar low energy conformer was found in the first set of calculations.

The structure in Fig. 6 is an energetically viable conformer for the peptide substrate assembled to the QD; however, it is important to note that the structure is also directed by several known parameters. Foremost, FRET measurements determined the position of the acceptor dye in the structure. FRET measurements in previous studies with peptides have also shown that QD-dye distances are consistent with binding of the full polyhistidine tract along the surface of the QD, without contribution to the overall separation; the PEG coating also prevents collapse of the peptide onto the QD surface and favors an extended conformation.[9, 15, 19, 23, 24] The known position of the acceptor dye relative to the QD is thus consistent with the expected kinked structure of the peptide [7, 8] following the extended polyproline spacer,[10] consistent with structures examined in the PDB. Although the peptide undoubtedly has some conformational freedom when bound to the QD, it is clear from the structural simulations that the trypsin can potentially have solution-like access to the arginine cleavage site.

Spectral Overlap Integrals

The qualitative spectral overlap between the QD donor emission and either the Cy3 or A594 acceptor absorption is shown in Fig. S4, along with the quantitative overlap functions.

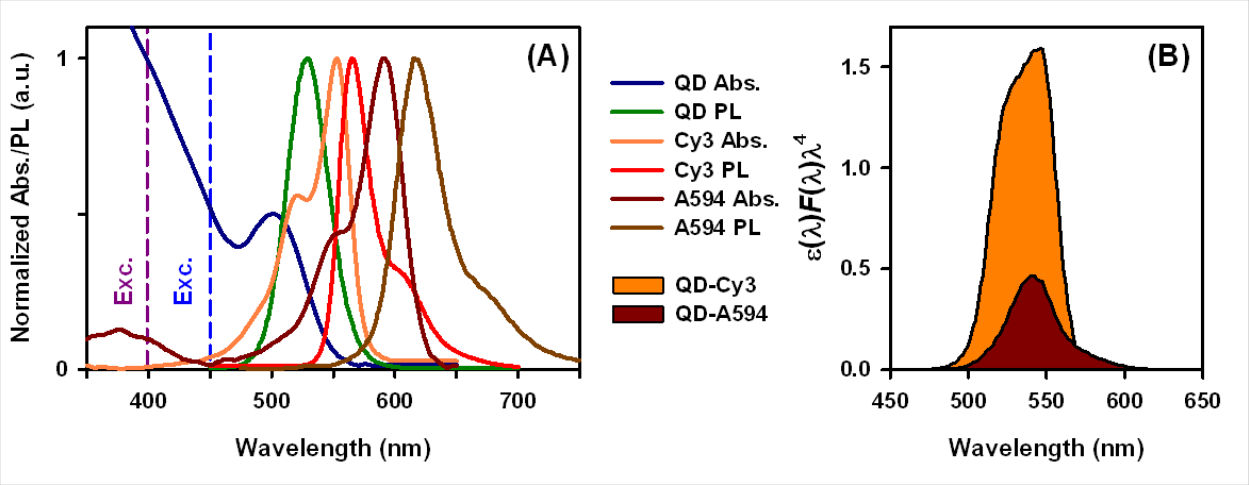

Figure S4. (A) Absorption and PL emission spectra for the QD donor, Cy3 acceptor, and A594 acceptor. The two excitation wavelengths used in this study are indicated. **(B)** The quantitative spectral overlap integrals for the QD-Cy3 and QD-A594 FRET pairs.

Validation with BANA substrate

MM plot analysis

PL intensity time courses for the evolution of 2-naphthylamine fluorescence during the hydrolysis of increasing concentrations of BANA by a fixed concentration of trypsin (*i.e.* classic MM plot assay format) are shown in Fig. S5A. The time-dependent calibration functions for samples of pre-hydrolyzed BANA (*i.e.* 2-naphthylamine) are shown in Fig. S5B.

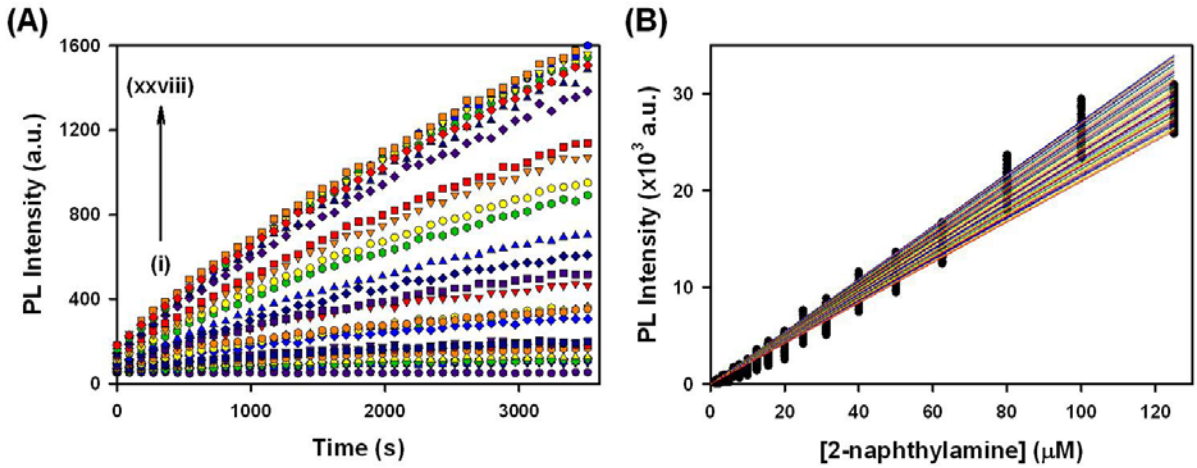

Figure S5. (A) Early time courses of 2-naphthylamine fluorescence intensity as a function of initial substrate concentration during digestion by 43 nM trypsin: (i) 0, (ii) 6.2, (iii) 7.0, (iv) 7.8, (v) 9.4, (vi) 12.5, (vii) 14.1, (viii) 15.6, (ix) 18.8, (x) 25.0, (xi) 28.1 (xii) 31.3, (xiii) 37.5, (xiv) 50.0, (xv) 56.3, (xvi) 62.5, (xvii) 75, (xviii) 100, (xix) 113, (xx) 125, (xxi) 150, (xxii) 200, (xxiii) 225, (xxiv) 250, (xxv) 300, (xxvi) 400, (xxvii) 450, and (xxviii) 500 μM BANA. **(B)** Time-dependent calibration plots for 2-naphthylamine (pre-hydrolyzed from BANA).

Kinetic analysis

PL intensity time courses for the evolution of 2-naphthylamine fluorescence during the hydrolysis of a fixed concentration of BANA by different concentrations of trypsin (*i.e.* kinetic assay format) are shown in Fig. S6A. The time-dependent calibration functions for samples of pre-hydrolyzed BANA (*i.e.* 2-naphthylamine) are shown in Fig. S6B. Analogous data for hydrolysis in the presence of QDs is shown in Fig. S6C-D. Fig. S6A shows the progress curves in terms of 2-naphthylamine product concentration for each experiment. The enzyme-time progress curve for the experiment with QDs is shown in Fig. S7B (analogous to Fig. 3B for the data without QDs). Large deviations from a common reaction trajectory (*i.e.* failing Selwyn's test) were observed for the hydrolysis of BANA by trypsin in the presence of 0.5 μM DHLA-PEG coated QDs.

Given the relatively low aqueous solubility of the BANA substrate, and the observation of a 2–fold increase in the BANA fluorescence in the presence of QDs, it likely that the BANA associated with the PEG coating of the QDs. At more than a 40-fold excess of BANA over QD, this would effectively create some degree of polyvalent QD-BANA substrate assembly,

suggesting potential similarity to the polyvalent QD-peptide conjugates that showed smaller deviations from Selwyn's test (*e.g.* Fig. 4D). Further analysis was hindered, however, by the absence of any of control over the substrate valence in the BANA system. Importantly, the QDs did not seem to induce a drastic increase or decrease in the net trypsin activity, despite apparent modification of the progress curve that likely relates to association between the QDs and trypsin, BANA substrate, and/or 2-naphthylamine product.

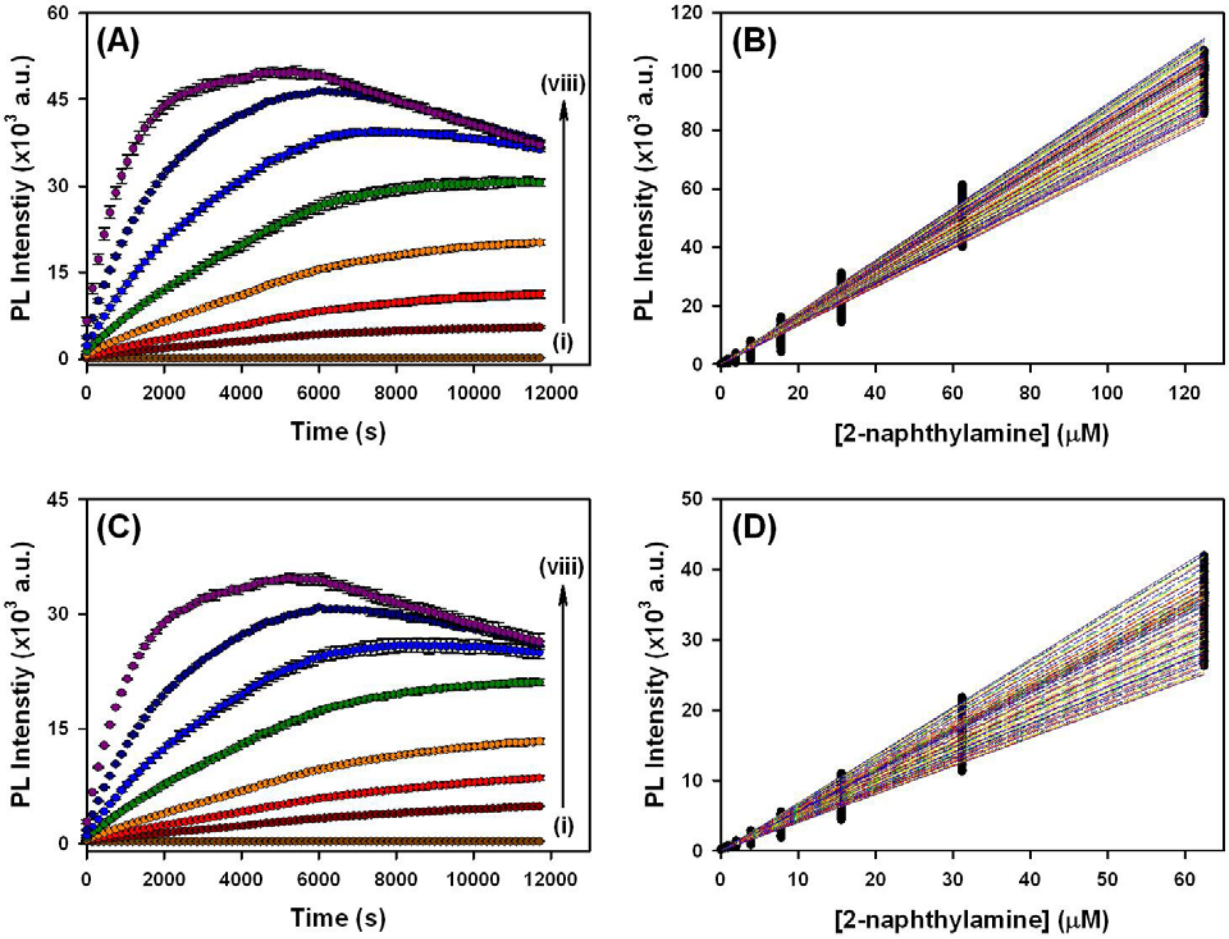

Figure S6. (A) Time-dependent 2-naphthylamine PL intensity (at 415 nm) during the hydrolysis of 58 μM BANA substrate by different concentrations of trypsin. **(B)** Time-dependent calibration plots for 2-naphthylamine (pre-hydrolyzed from BANA). **(C)** Time-dependent 2-naphthylamine PL intensity (at 415 nm) during the hydrolysis of BANA substrate by different concentrations of trypsin in the presence of 0.5 μM DHLA-PEG coated QDs. **(D)** Time-dependent calibration plots for 2-naphthylamine (pre-hydrolyzed from BANA) in the presence of 0.5 μM DHLA-PEG coated QDs. The trypsin concentrations in A and B were: (i) 0, (ii) 0.04, (iii) 0.09, (iv) 0.17, (v) 0.34, (vi) 0.69, (vii) 1.37 and (viii) 2.75 μM. The slope of the calibration curves decreased with increasing time.

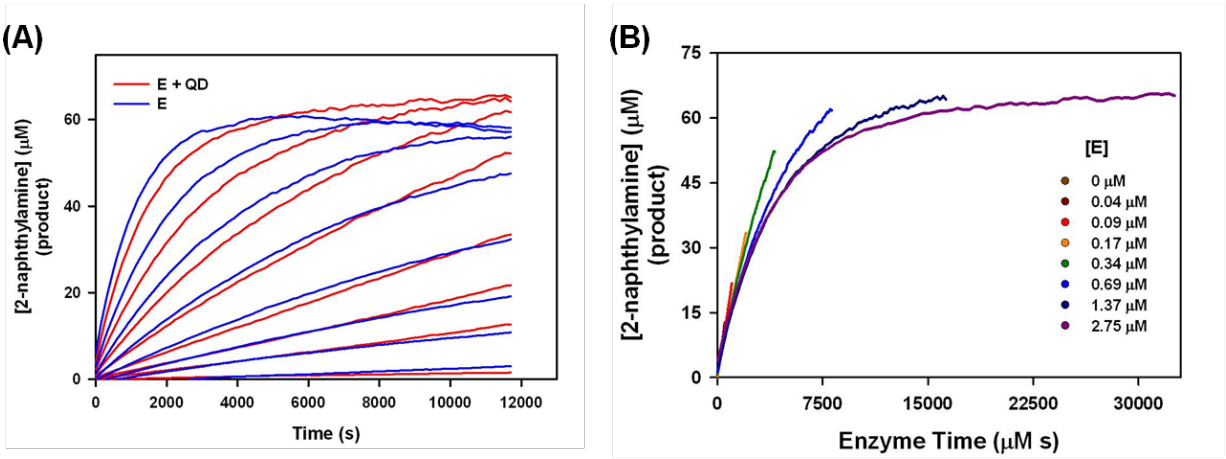

Figure S7. (A) Progress curves for BANA substrate (58 μM) hydrolysis by trypsin (E) and trypsin in the presence of 0.5 M DHLA-PEG coated QDs (E + QD). The trypsin concentrations were: (i) 0, (ii) 0.04, (iii) 0.09, (iv) 0.17, (v) 0.34, (vi) 0.69, (vii) 1.37 and (viii) 2.75 μM. **(B)** BANA substrate hydrolysis progress curves in the presence of 0.5 μM DHLA-PEG coated QDs as product concentration *versus* enzyme-time. Note that the data for the different trypsin concentrations, [E], are not superimposed.

Non-specific adsorption and FRET calibration curves

The measured A/D PL ratios for tryptic QD-peptide conjugate digestions done at the three highest trypsin concentrations generally converged to a common endpoint; however, these end-points were non-zero. This observation was in direct contrast to the approximately zero endpoint expected for complete cleavage of the peptide substrates from the QDs, and was observed with all of the QD-(peptide-Cy3)$_n$ conjugates (n = 2.4, 3.7, 7.0) and the QD-(peptide-A594)$_{13.4}$ conjugate. The residual A/D PL ratio increased with increasing conjugate valence, and was especially large for the QD-(peptide-A594)$_{13}$ conjugates. Accordingly, the use of only the native peptide (*i.e.* substrate) calibration curves in Fig. 2 was insufficient. When used to convert the kinetic FRET data into kinetic data for the peptide substrate conjugate valence, these functions returned progress curves that did not approach zero, preventing reliable determination of enzyme kinetic parameters.

To rationalize the above results, A594-labeled peptide substrate in bulk solution was digested with trypsin in the absence of QDs. Polyacrylamide gel electrophoresis (Fig. S8A) showed two resolved bands for the native peptide substrate and digested peptide product, with no indication of a large, residual undigested peptide population. QD-(peptide-A594)$_{13.4}$ conjugates were then digested with trypsin for an extended period and analyzed by agarose gel electrophoresis (Fig. S8B). The DHLA-PEG coated QDs had minimal electrophoretic mobility. Conjugation of the native peptide substrate to the QD moderately increased its mobility, and this was likely due to the anionic character of the A594 dye and peptide. The QD and A594 PL were co-localized within the single band. Digestion of the QD-peptide substrate conjugate yielded a decrease in QD mobility and the appearance of a second band with greater mobility. This latter band was exclusively associated with A594 PL, and corresponded to the peptide product fragment, A594-CSTR. The co-localization of QD and A594 in the lower mobility band was significantly decreased. The misalignment of the QD PL and the residual A594 PL was consistent with non-

specific adsorption of some of the A594-labeled peptide product fragment and slow desorption under the applied electric field.

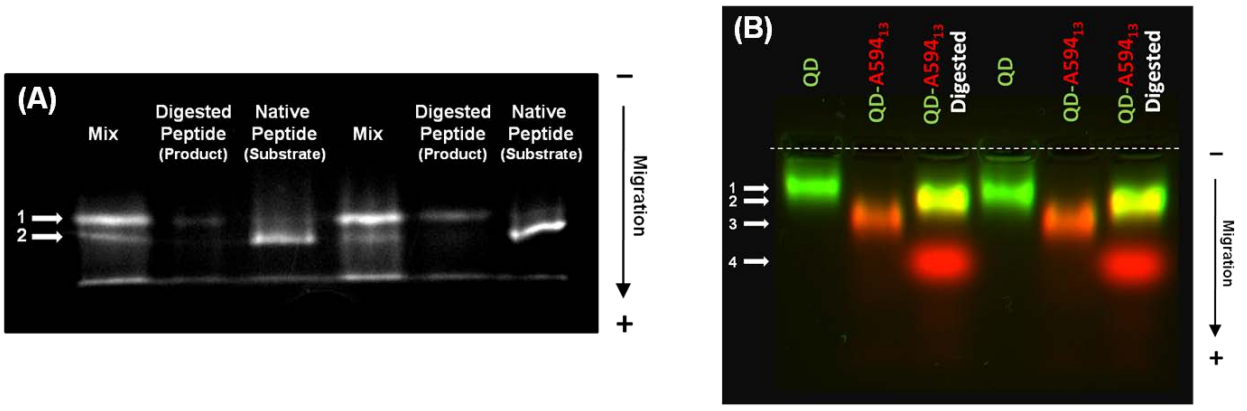

Figure S8. (A) Gradient polyacrylamide gel electrophoresis of the A594-labeled substrate peptide, with and without tryptic digestion. The arrows indicate the bands corresponding to (1) digested peptide and (2) native substrate peptide. The lower line across the bottom is the end of the gel. **(B)** Agarose gel electrophoresis of QD-(peptide-A594)$_{13}$ conjugates. The arrows at the left indicate the position of the bands associated with: (1) DHLA-PEG QDs, (2) digested QD-(peptide-A594)$_{13}$ conjugates, (3) native QD-(peptide-A594)$_{13}$ conjugates, and (4) the A594-labeled product peptide fragment. The gel image is pseudocolored, where green predominately reflects QD PL and red predominately reflects A594 PL.

Given the large difference in residual FRET signal between tryptic digests of QD-(peptide-Cy3)$_n$ and QD-(peptide-A594)$_{13.4}$ conjugates, the adsorption was likely mediated by interactions with the acceptor dye. The greater affinity of the A594 dye toward the QD surface is also a probable cause of the slightly shorter donor-acceptor distance measured for A594-labeled peptide substrate compared to the use of Cy3-labeled peptide. In order to quantitatively assess dye-labeled product adsorption, the QDs were mixed with increasing amounts of pre-digested Cy3- and A594-labeled peptide product fragments, and the PL spectra measured to estimate the FRET resulting from non-specific adsorption. This is shown in parallel with the assembly of native substrate peptide in Fig. 2. The A/D PL ratios corresponding to the various target conjugate valences (N = 2, 4, or 8 digested Cy3 per QD, and N = 12 digested A594 per QD) were in good agreement with the residual signals at the end of the kinetic measurements of the different trypsin digests: 0.06 *vs.* 0.08 for the QD-(peptide-Cy3)$_{2.4}$, 0.13 *vs.* 0.14 for the QD-(peptide-Cy3)$_{3.7}$, 0.27 *vs.* 0.28 for the QD-(peptide-Cy3)$_{7.0}$, and 1.2 *vs.* 1.4 for the QD-(peptide-A594)$_{13.4}$. Clearly, the adsorption of dye-labeled product to the QD was the cause of the non-zero FRET residuals after complete digestion of the peptide substrates.

To fully account for non-specific adsorption in our kinetic analysis, new calibration curves were constructed for *each* proteolysis experiment by mathematically adding the A/D PL ratios for the adsorption of Cy3/A594-labeled peptide product fragments to that for the Cy3/A594-labeled peptide substrate bound through the polyhistidine motif. In the case of the QD-(peptide-Cy3)$_2$ conjugates, this was a three-point calibration with 2:0, 1:1, and 0:2 ratios of substrate and pre-digested product peptide. In general, for QD-(peptide-dye)$_N$ conjugates, the calibration points were N:0, (N-1):1, (N-2):2 … 2:(N-2), 1:(N-1), and 0:n ratios. This procedure worked well for the

QD-(peptide-Cy3)$_n$ conjugates, where the calibration functions for $N = 2$, 4 and 8 (Fig. S9) converted Cy3/QD PL ratio data into kinetic data with conjugate valences that approached zero.

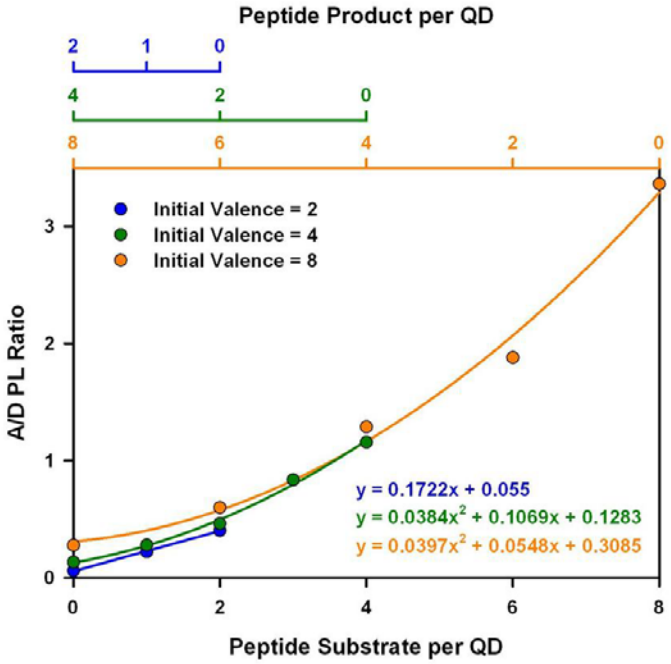

Figure S9. Calibration functions for QD-(peptide-Cy3)$_N$ conjugates (N = 2, 4 and 8) that account for bound Cy3-labeled peptide substrate and adsorbed Cy3-labeled peptide product fragments. The curves are constructed from the sum of the appropriate points on the curve in Fig. 2A(iii).

Unfortunately, it was found that this mathematical addition of the calibration signals for bound peptide substrates and adsorbed peptide product fragments was unsuitable with the A594 dye, yielding impossibly high FRET efficiencies and a pronounced distortion of the kinetic traces for the QD-(peptide-A594)$_{13}$ conjugates. Rather, the appropriate calibration was constructed experimentally by mixing different amounts of A594-labeled substrate and pre-digested product peptides at the ratios noted above. The resulting mixed calibration curve is shown in Fig. 2B(iii), where the dual convergence with the curves for only native peptide (substrate) and only digested peptide (product) should be noted. Use of the mixed calibration curve to convert A594/QD PL ratio data into kinetic data for conjugate valence, yielded progress curves that nearly approached zero at the end of the digest.

The experimental measurement of non-specific adsorption was one of several control experiments and calibrations needed to access quantitative information. This accounting also included QD and dye emission crosstalk, direct excitation of the acceptor dye, and instrumental drift. In general, it appears that the non-specific adsorption of labeled peptide product warrants particular attention; its magnitude appears to be a function of the QD coating and dye selection in this work, but could conceivably also be a function of the nature of the enzymatic product in other systems. As a further complication, the experiments with the A594-labeled peptide clearly demonstrated that the residual substrate and product fragments bound to a QD can potentially play a role a determining the ability of the labeled product fragment to adsorb. Strong and weak

adsorption may also need to be accounted for differently, as we found with the A594- and Cy3-labeled peptides. These are design considerations and checks that can be done prior to enzyme assays, permitting the case-by-case optimization of assay formats.

Digestion of Peptide Substrates and Kinetic Analysis

In addition to kinetic monitoring of QD-peptide substrate conjugate digestion, attempts were made to monitor the digestion of only peptide substrate. A peptide was synthesized with the substrate sequence CSTRIDEANQAATSLP$_7$SK(Texas Red)H$_6$ and subsequently labeled at the cysteine residue using Cy3 maleimide. It was intended that the Cy3 and Texas Red would act as a donor-acceptor FRET pair and enable ratiometric detection of proteolysis without a QD donor nano-platform. However, it became apparent that the Cy3 and Texas Red formed a biomolecular complex with photophysical properties (*e.g.* exciton coupling) that were very different than the original dyes, and which precluded quantitative FRET-based measurements. Trypsin was unable to appreciably disrupt the aqueous complex, which was largely (but not fully) dissociated in 70% acetonitrile. Mixing equimolar quantities of two different peptides labeled separately with Cy3 and Texas Red did not result in complex formation, suggesting that Cy3-Texas Red complex formation was favored by the close proximity induced by labeling at two sites along a common peptide backbone. Similar observations were made when the Cy3 was replaced with Alexa Fluor 555 (a spectral analog with a different molecular structure and good aqueous solubility).

Digestion of Peptide Substrates and a Classic MM Plot

Fig. S10 shows the assay and calibration data for determination of the peptide substrate kinetic parameters using a classic excess substrate MM plot format. Note the convergence of the fluorescence from calibration and assay samples at low initial substrate concentrations, and the departure as the initial substrate concentration is increased and *V* is approached.

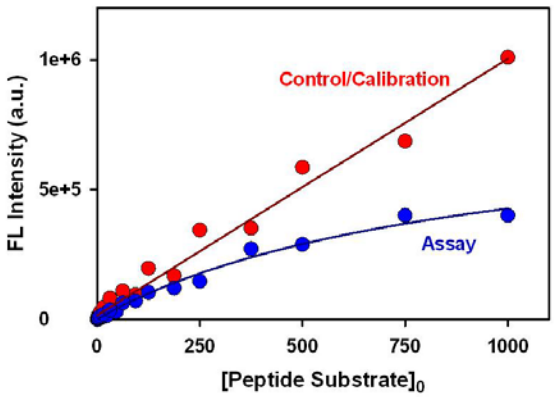

Figure S10. Calibration and proteolysis data for the peptide substrate in a classic MM plot assay using excess substrate and a fixed concentration of trypsin.

Digestion of Quantum Dot-Peptide Substrate Conjugates

The basis of our ratiometric, FRET-based, kinetic assay was the rapid measurement of changes in QD and Cy3/A594 acceptor PL intensity during proteolysis. Although the PL emission spectra of the QD and Cy3 were largely resolved, there was nonetheless some residual overlap. Real-time monitoring of proteolysis requires data acquisition to be fast compared to the interval between measurement points. Unfortunately, the acquisition of full spectra would have required minutes per sample, which is too long of an interval for kinetic measurements—each sample would have been measured at a distinctly different point in the reaction, and the D/A contributions to each spectrum might have changed non-trivially during their acquisition. Instead, nearly concurrent measurements of QD and Cy3/A594 PL was achieved by serial measurement of the PL intensity at two wavelengths: the QD PL maximum (530 nm), and near either the Cy3 (575 nm) or A594 (617 nm) PL maximum. The timescale of these measurements were on the order of seconds. Data acquired in calibration experiments were then used to estimate correction factors that served analogously to deconvolution, providing an accurate A/D PL intensity ratio. Importantly, ratiometric measurements are relatively insensitive to both dilution and small variations in experimental format (*e.g.* excitation intensity, detector gain). This allows samples to be measured independently of each other, and is particularly well suited to kinetic assays where PL is constantly changing over ≥ 2 h.[2]

In our assays, the $[S]_0/[E]_0$ ratio was always >10 for the conjugate valence $n = 13.4$, and for $n = 7.0$ the ratio was >10 for all but the highest trypsin concentration used. Although the two highest trypsin concentrations for $n = 3.7$ and $n = 2.4$ were only in slight excess ($[S]_0/[E]_0 \approx 3–6$), half of the progress curves obtained at each conjugate valence were at $[S]_0/[E]_0 > 100$. Further, the highest trypsin concentration used was also >100-fold less than the K_m value associated with the peptide substrate. These conditions are such that use of the Briggs-Haldane assumption and MM model should be approximately valid without complications from other sources (*e.g.* QDs).

Figs. S11–S14 show the stepwise conversion of real-time, two-color PL time courses into tryptic digestion progress curves in terms of conjugate valences and bulk substrate concentration. Note that the progress curves are collected over *ca.* 2.5 h. In general, we suggest that tuning of enzyme activity *via* experimental conditions (*e.g.*, enzyme and substrate concentration, pH, divalent cations, or temperature) may be necessary to obtain a useful compromise between sufficient temporal resolution and reasonable durations of progress curves within the limitations of available instrumentation. Optimization of experimental parameters may also facilitate working at very large excesses of one or more components (*e.g.* substrate) so that quantitative modeling and analysis is simplified. It is worthwhile to note that the self-assembly of peptides to QDs follows a Poisson distribution, where the targeted average valence is approximately reflected across individual QDs in the ensemble as $N \rightarrow 4$.[25] In the case of $n = 2.4$, the individual QDs tend to have a range of conjugate valences that average out to this value. However, this factor is only a challenge in determining accurate FRET efficiencies and is circumvented by the empirical calibration using A/D PL ratios. We also neglect the effects of the low valence Poisson distribution on proteolysis which are expected to be small.[15]

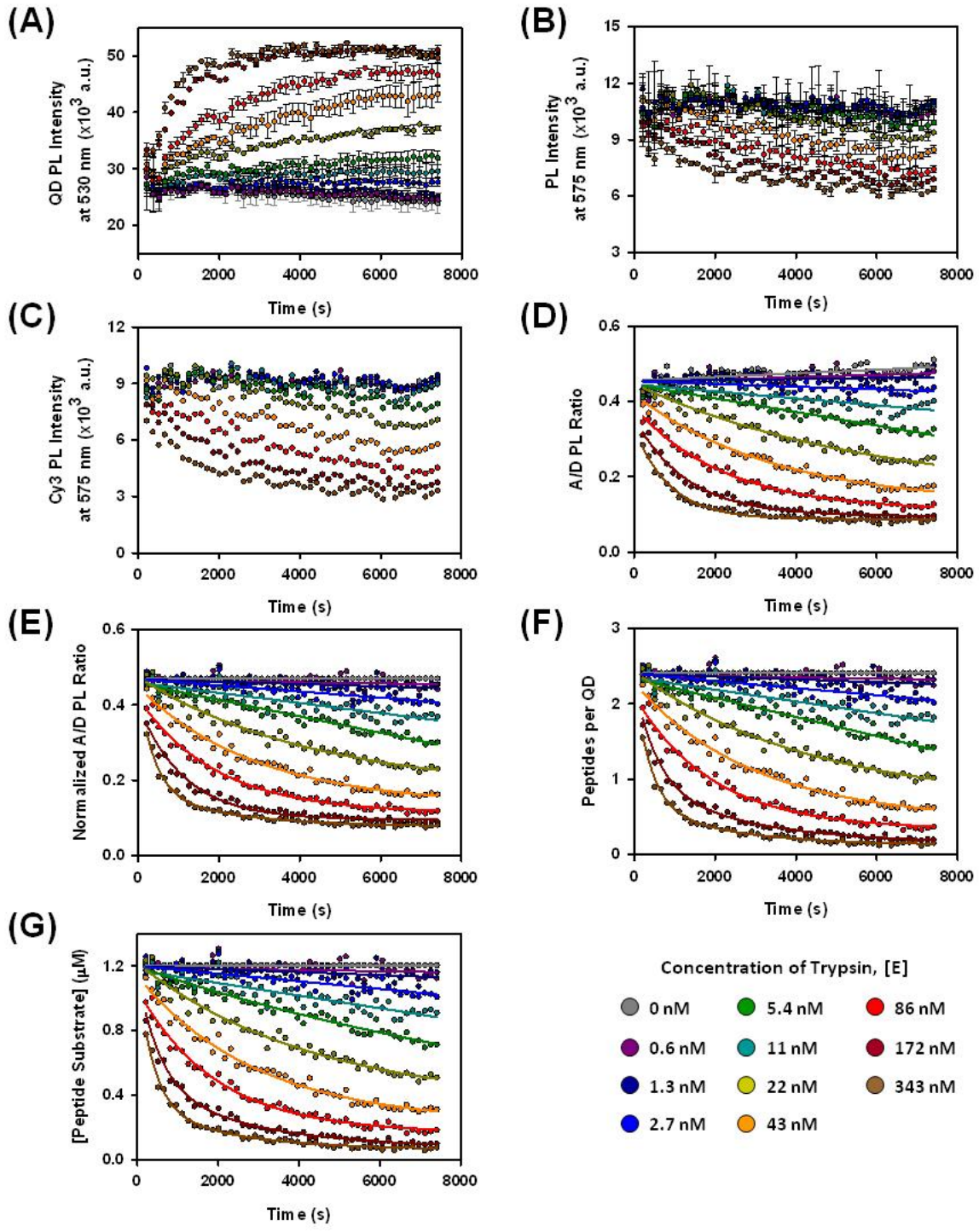

Figure S11. Two-color proteolytic reaction progress curve data and analysis for **QD-(peptide-Cy3)$_{2.4}$** conjugates: **(A)** QD PL signal; **(B)** uncorrected Cy3 PL signal; **(C)** corrected Cy3 PL signal; **(D)** A/D PL ratio; **(E)** normalized A/D PL ratio; **(F)** QD-peptide substrate conjugate valence; and **(G)** total concentration of peptide substrate.

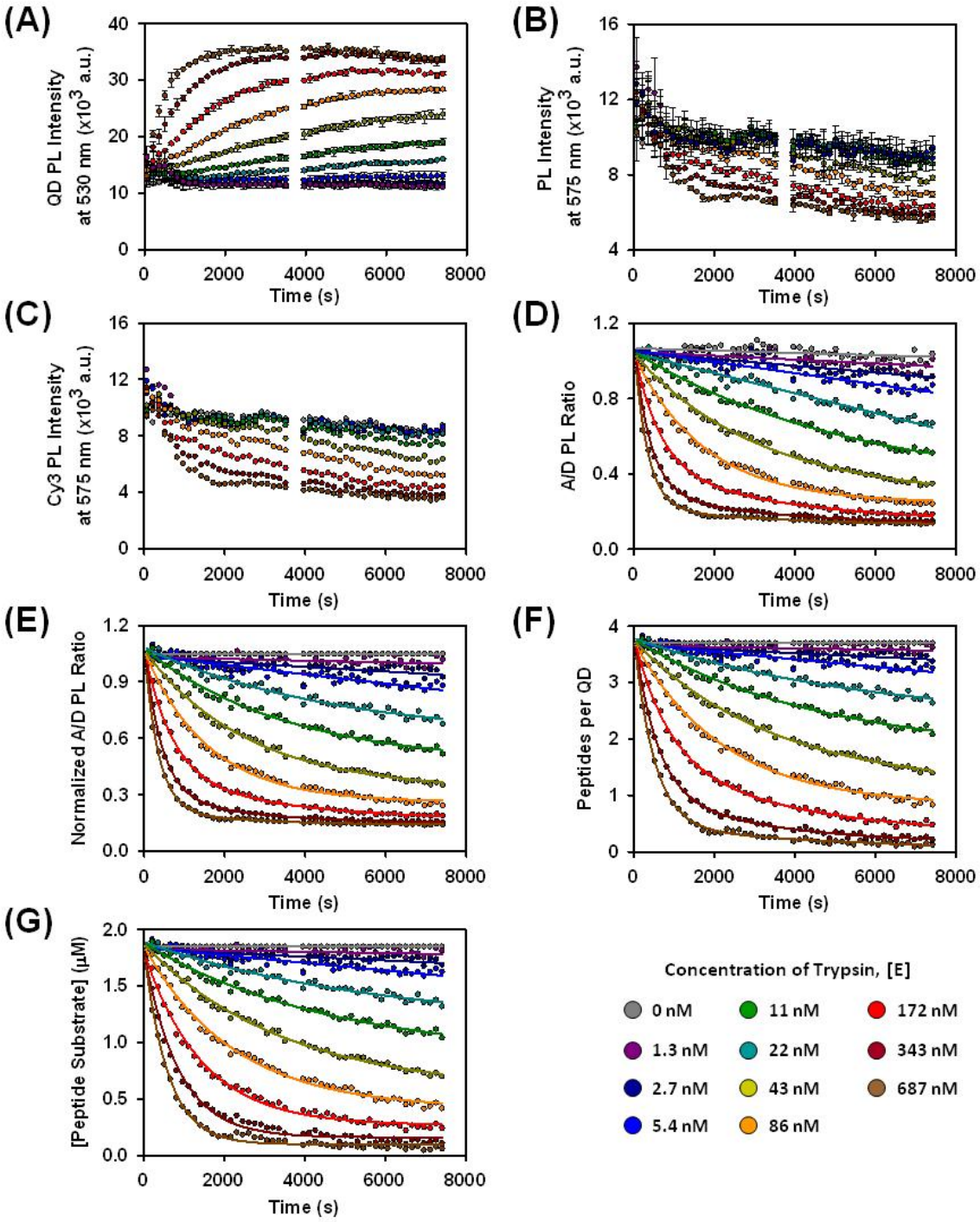

Figure S12. Two-color proteolytic reaction progress curve data and analysis for **QD-(peptide-Cy3)$_{3.7}$** conjugates: **(A)** QD PL signal; **(B)** uncorrected Cy3 PL signal; **(C)** corrected Cy3 PL signal; **(D)** A/D PL ratio; **(E)** normalized A/D PL ratio; **(F)** QD-peptide substrate conjugate valence; and **(G)** total concentration of peptide substrate. The missing data points at ~3750 s are due to a power flicker during the experiment.

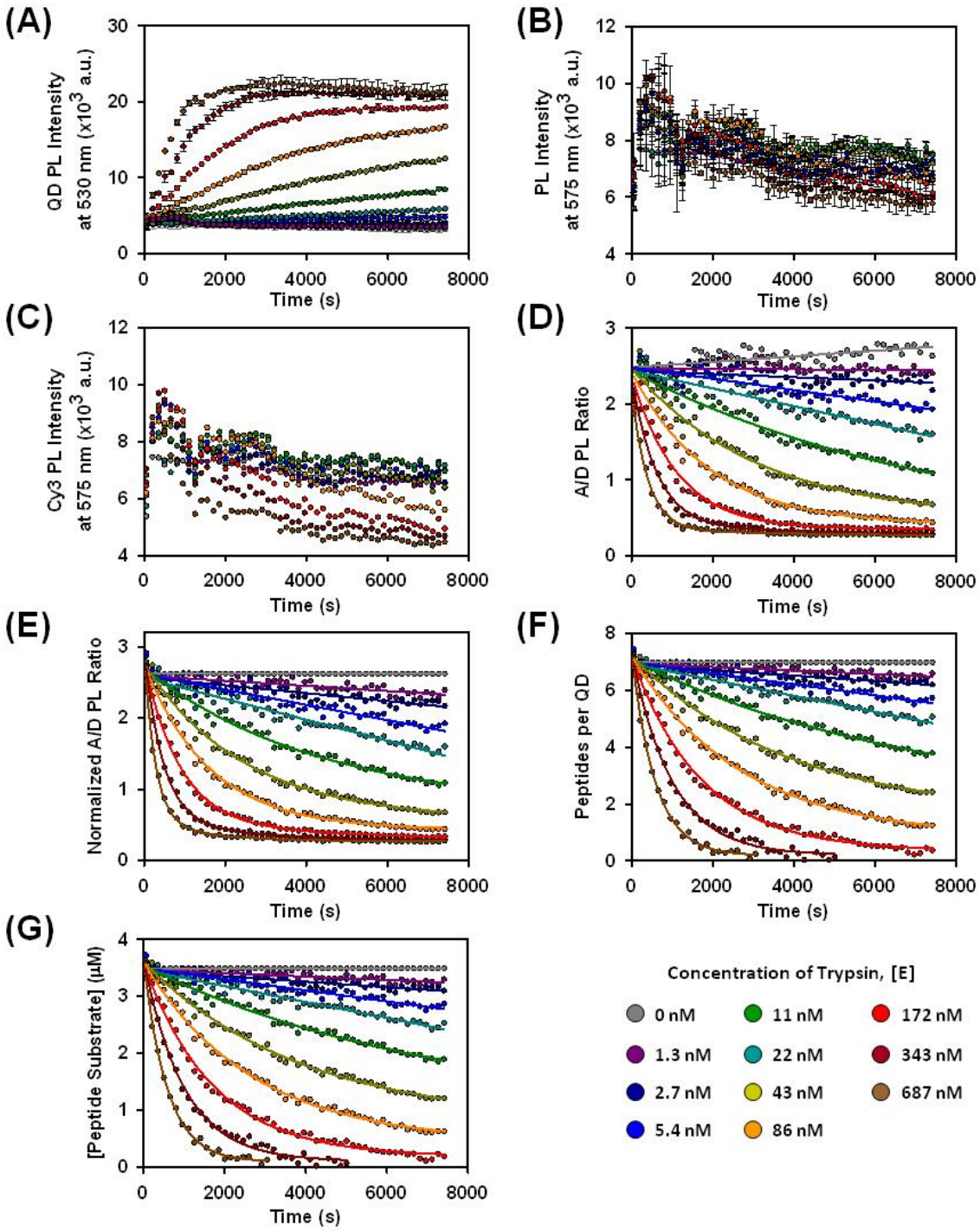

Figure S13. Two-color proteolytic reaction progress curve data and analysis for **QD-(peptide-Cy3)$_{7.0}$** conjugates: **(A)** QD PL signal; **(B)** uncorrected Cy3 PL signal; **(C)** corrected Cy3 PL signal; **(D)** A/D PL ratio; **(E)** normalized A/D PL ratio; **(F)** QD-peptide substrate conjugate valence; and **(G)** total concentration of peptide substrate.

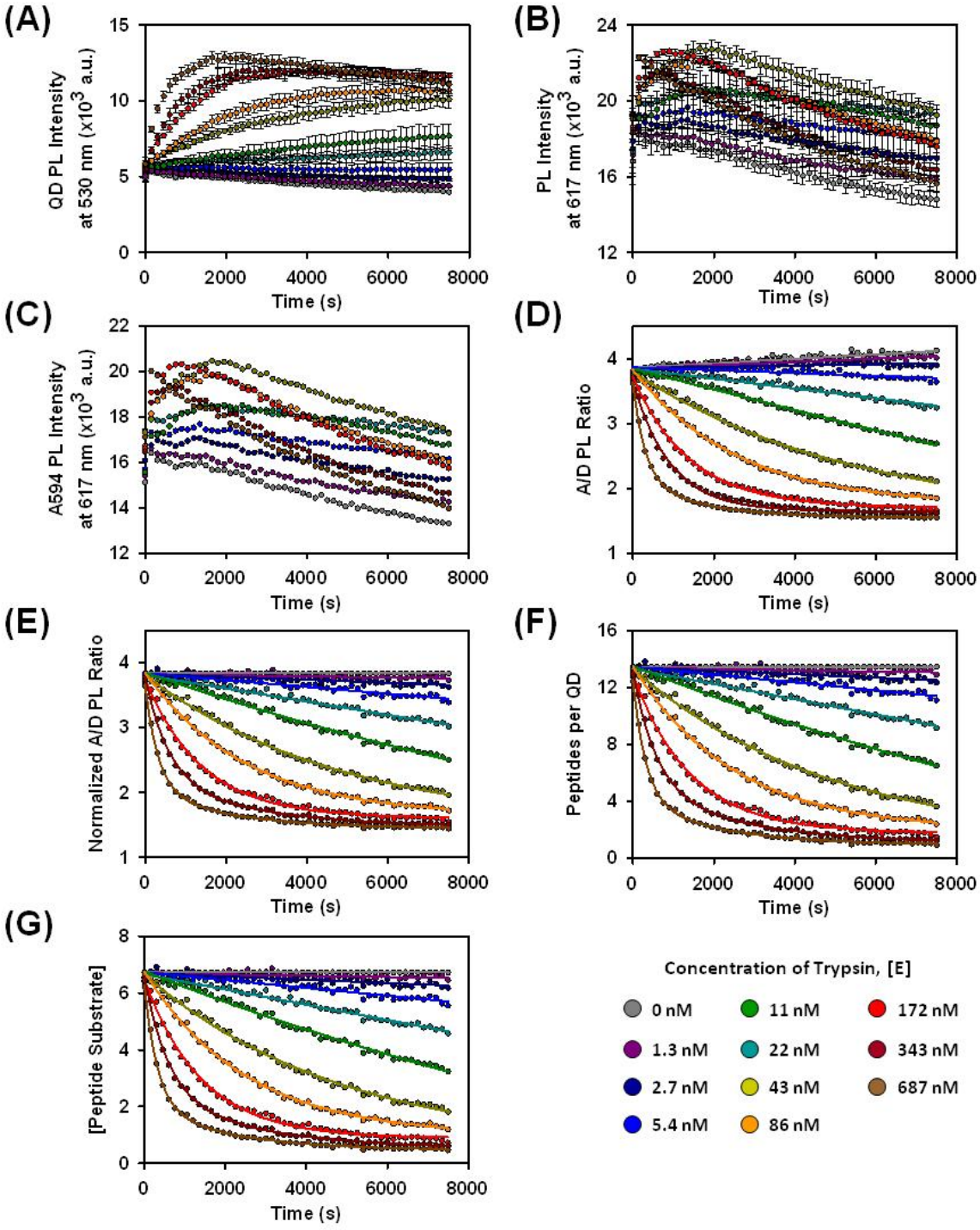

Figure S14. Two-color proteolytic reaction progress curve data and analysis for **QD-(peptide-A594)$_{13.4}$** conjugates: **(A)** QD PL signal; **(B)** uncorrected A594 PL signal; **(C)** corrected A594 PL signal; **(D)** A/D PL ratio; **(E)** normalized A/D PL ratio; **(F)** QD-peptide substrate conjugate valence; and **(G)** total concentration of peptide substrate.

References

1. Sapsford, K. E.; Farrell, D.; Sun, S.; Rasooly, A.; Mattoussi, H.; Medintz, I. L. *Sens Actuat B Chem* **2009,** 139, 13-21.
2. Lakowicz, J. R., *Principles of Fluorescence Spectroscopy*. 3rd ed.; Springer: New York, 2006.
3. Clapp, A. R.; Medintz, I. L.; Mauro, J. M.; Fisher, B. R.; Bawendi, M. G.; Mattoussi, H. *J Am Chem Soc* **2004,** 126, 301-310.
4. Luo, G.; Wang, M.; Konigsberg, W. H.; Xie, X. S. *Proc Natl Acad Sci USA* **2007,** 104, 12610-12615.
5. Goličnik, M. *Anal Biochem* **2010,** 406, 94-96.
6. Goličnik, M. *Anal Biochem* **2011,** 411, 303-305.
7. Breidenbach, M. A.; Brunger, A. T. *Nature* **2004,** 432, 925-929.
8. Fu, Z.; Chen, S.; Bladwin, M. R.; Boldt, G. E.; Crawford, A.; Janda, K. D.; Barbieri, J. T.; Kim, J.-J. P. *Biochem* **2006,** 45, 8903-8911.
9. Sapsford, K. E.; Granek, J.; Deschamps, J. R.; Boeneman, K.; Blanco-Canosa, J. B.; Dawson, P. E.; Susumu, K.; Stewart, M. H.; Medintz, I. L. *ACS Nano* **2011,** 5, 2687-2699.
10. Shi, Z. S.; Olson, C. A.; Bell, A. J.; Kallenbach, N. R. *Biopolymers* **2001,** 60, 366-380.
11. Pettersen, E. F.; Goddard, T. D.; Huang, C. C.; Couch, G. S.; Greenblatt, D. M.; Meng, E. C.; Ferrin, T. E. *J Comput Chem* **2004,** 25, 1605-1612.
12. Medintz, I. L.; Pons, T.; Susumu, K.; Boeneman, K.; Dennis, A. M.; Farrell, D.; Deschamps, J. R.; Melinger, J. S.; Bao, G.; Matoussi, H. *J Phys Chem C* **2009,** 113, 18552-18561.
13. Boeneman, K.; Mei, B. C.; Dennis, A. M.; Bao, G.; Deschamps, J. R.; Mattoussi, H.; Medintz, I. L. *J Am Chem Soc* **2009,** 131, 3838-3829.
14. Prasuhn, D. E.; Deschamps, J. R.; Susumu, K.; Stewart, M. A.; Boeneman, K.; Blanco-Canosa, J. B.; Dawson, P. E.; Medintz, I. L. *Small* **2009,** 6, 555-564.
15. Medintz, I. L.; Clapp, A. R.; Brunel, F. M.; Tiefenbrunn, T.; Uyeda, H. T.; Chang, E. L.; Deschamps, J. R.; Dawson, P. E.; Mattoussi, H. *Nat Mater* **2006,** 5, 581-589.
16. Goldman, E. R.; Medintz, I. L.; Whitley, J. L.; Hayhurst, A.; Clapp, A. R.; Uyeda, H. T.; Deschamps, J. R.; Lassman, M. E.; Mattoussi, H. *J Am Chem Soc* **2005,** 127, 6744-6751.
17. Medintz, I. L.; Clapp, A. R.; Melinger, J. S.; Deschamps, J. R.; Mattoussi, H. *Adv Mater* **2005,** 17, 2450-2455.
18. Medintz, I. L.; Konnert, J. H.; Clapp, A. R.; Stanish, I.; Twigg, M. E.; Matoussi, H. *Proc Natl Acad Sci USA* **2004,** 101, 9612-9617.

19. Boeneman, K.; Deschamps, J. R.; Buckhout-White, S.; Prasuhn, D. E.; Blanco-Canosa, J. B.; Dawson, P. E.; Stewart, M. H.; Susumu, K.; Goldman, E. R.; Ancona, M.; Medintz, I. L. *ACS Nano* **2010,** 4, 7253-7266.

20. Wang, J.; Wang, W.; Kollman, P. A.; Case, D. A. *J Mol Graphics* **2006,** 25, 247-260.

21. Ibrahim, B. S.; Pattanhi, V. *J Mol Biol* **2005,** 348, 1191-1198.

22. Li, J.; Zhang, C.; Xu, X.; Wang, J.; Yang, H.; Xu, C.; Ma, D.; Wang, Y.; Gong, W.; Lai, R., doi:10.2210/pdb2o9q/pdb.

23. Prasuhn, D. E.; Feltz, A.; Blanco-Canosa, J. B.; Susumu, K.; Stewart, M. H.; Mei, B. C.; Yakovlev, A. V.; Loukov, C.; Mallet, J. M.; Oheim, M.; Dawson, P. E.; Medintz, I. L. *ACS Nano* **2010,** 4, 5487-5497.

24. Prasuhn, D. E.; Blanco-Canosa, J. B.; Vora, G. J.; Delehanty, J. B.; Susumu, K.; Mei, B. C.; Dawson, P. E.; Medintz, I. L. *ACS Nano* **2010,** 4, 267-278.

25. Pons, T.; Medintz, I. L.; Wang, X.; English, D. S.; Mattoussi, H. *J Am Chem Soc* **2006,** 128, 15324-15331.